Fuel 225 (2018) 403–410

Contents lists available at ScienceDirect

Fuel

journal homepage: www.elsevier.com/locate/fuel

Full Length Article

Nanostructured molybdenum carbide on biochar for CO_2 reforming of CH_4

Rui Li[a], Abolghasem Shahbazi[a,*], Lijun Wang[a], Bo Zhang[a], Ching-Chang Chung[b], David Dayton[c], Qiangu Yan[d,*]

[a] Department of Natural Resources and Environmental Design, North Carolina A & T State University, Greensboro, NC 27411, United States
[b] Department of Materials Science and Engineering, North Carolina State University, Raleigh, NC 27695, United States
[c] Energy Technology Division, RTI International, Research Triangle Park, Durham, NC 27709, United States
[d] Department of Sustainable Bioproducts, Mississippi State University, Mississippi, MS 39762, United States

GRAPHICAL ABSTRACT

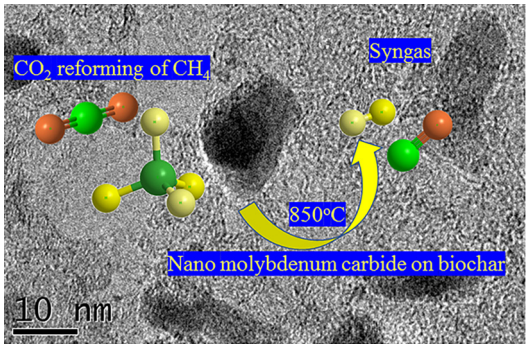

ARTICLE INFO

Keywords:
Molybdenum carbide
In-situ XRD
CO_2 reforming of CH_4
Temperature programmed surface reactions
Thermodynamic analysis

ABSTRACT

A simple procedure was developed to synthesize molybdenum carbide nanoparticles (Mo_2C/BC) by carburization of molybdate salts supported on the biochar from pyrolysis of biomass without using extra carbon source or reducing gas. The molybdenum carbide formation procedure investigated by *in-situ* XRD and TGA-MS indicated that the phase transitions followed the path of $(NH_4)_6Mo_7O_{24}{\cdot}4H_2O \rightarrow (NH_4)_2Mo_3O_{10} \rightarrow (NH_4)_2Mo_{14}O_{42} \rightarrow Mo_8O_{23} \rightarrow Mo_4O_{11} \rightarrow MoO_2 \rightarrow Mo_2C$. The volatile gases CO, H_2, and CH_4 evolved from biochar and the biochar solid carbon participated in the reduction of molybdenum species, while the biochar and CH_4 served as carbon sources for the carburization.

Temperature programmed surface reactions of Mo_2C/BC indicated that CH_4 dissociated as $CH_4 \leftrightharpoons C* + 2H_2$ on the catalyst surface, and CO_2 reacted as $CO_2 + C* \leftrightharpoons 2CO + *$ due to oxidation of Mo_2C. Both experiment data and thermodynamic analysis for the study of operation conditions of CO_2 reforming of CH_4 clearly demonstrated that the yields of H_2 and CO increased with the increased temperature and the reasonable conversions should be performed at 850 °C, at which both CH_4 and CO_2 conversions were higher than 80%.

1. Introduction

Carbon dioxide (CO_2) reforming of methane (CH_4) reaction (i.e., dry reforming of CH_4, DRM), which converts two greenhouse gases into syngas (CO and H_2), is a very promising technology for both industrial production and environmental impacts. The CO_2 reforming of CH_4

* Corresponding authors at: Department of Natural Resources and Environmental Design, North Carolina A & T State University, NC, United States (A. Shahbazi) and Department of Sustainable Bioproducts, Mississippi State University, Mississippi, MS 39762, United States (Q. Yan).
E-mail addresses: ash@ncat.edu (A. Shahbazi), yanqiangu@gmail.com (Q. Yan).

https://doi.org/10.1016/j.fuel.2018.03.179
Received 11 January 2018; Received in revised form 26 March 2018; Accepted 28 March 2018
Available online 02 April 2018
0016-2361/

Table 1
Thermodynamic analysis of related in the CO_2 reforming of CH_4.

Reaction	Equation	ΔH°_{298} (kJ/mol)	$\Delta G^{\circ} \leq 0$, T(°C)
CO_2 reforming of CH_4	$CH_4(g) + CO_2(g) = 2CO(g) + 2H_2(g)$	247	≥643
Reverse water gas shift	$CO_2(g) + H_2(g) = CO(g) + H_2O(g)$	41	≥817
Boudouard reaction	$2CO(g) = CO_2(g) + C(s)$	−172	≤700
Methane decomposition	$CH_4(g) = 2H_2(g) + C(s)$	75	≥547
Steam reforming reaction	$CH_4(g) + H_2O(g) = CO(g) + 3H_2(g)$	206	≤620

reaction is always accompanied by several side reactions, including reverse water–gas shift reaction (RWGS), Boudouard reaction, methane decomposition, and steam reforming reaction. As shown in Table 1, the enthalpy of CO_2 reforming of CH_4 is 247 kJ/mol and the equilibrium state temperature for $\Delta G \leq 0$ is $T \geq 643$ °C, which indicates the CO_2 reforming of CH_4 reaction is highly endothermic and happening over 643 °C. The reverse water–gas shift reaction consumes CO_2 and H_2, and produces CO and H_2O. The side reactions related to carbon formation include Boudouard reaction and methane decomposition. Methane decomposition is slightly endothermic and occurs over 547 °C, and Boudouard reaction is moderately exothermic and occurs below 700 °C. Hence, carbon formation takes place significantly between 547 and 700 °C. In addition, the variation of Gibbs free energy with temperature was plotted in Fig. S1. It clearly exhibited that CO_2 reforming of CH_4 reaction always occurred with steam reforming reaction and methane decomposition reaction over 643 °C. So, carbon deposition cannot be avoided due to methane decomposition. Between 700 and 817 °C, only CO_2 reforming of CH_4 reaction, steam reforming reaction, and methane decomposition reaction occurred. Over 817 °C, only Boudouard reaction of them did not take place.

Up to date, the most studied catalysts for DRM were nickel-based catalysts, which have been limited in industrial applications [1], because they were susceptible to deactivation due to the deposition of carbon. To further commercialize the DRM process, a high coking resistance catalyst is decidedly needed [2]. Molybdenum carbide is particularly interesting to CO_2 conversion because of its excellent coke resistance [3–5], high sulfur tolerance, and potential to behave similarly to reducible oxides [6,7]. Although transition metal carbide catalysts may be rapidly deactivated by CO_2 at an atmospheric pressure due to the oxidation of catalysts [8,9], the molybdenum carbide catalysts can exhibit stable activity at an elevated pressure (e.g., 0.83 MPa) at 847 °C [3]. Therefore, part of this work is to investigate the oxidation-carburization reaction on molybdenum carbide during the DRM reaction.

The conventional method for synthesizing carbides is carbothermal hydrogen reduction, which uses a gaseous carbon source (like CH_4) and a reducing agent (like H_2). But recent research has shown growing interest to synthesize molybdenum carbide without using any gaseous carbon source, i.e., using a solid carbon material alone such as carbon nanotubes [10,11], carbon black [11], cedar wood [12] and sawdust [13]. Synthesis of carbides on biochar without using any gaseous carbon source has been demonstrated on tungsten carbide [14] and iron carbide [15]. Biochar is a solid byproduct of fast pyrolysis of lignocellulosic biomass, which is a low-cost carbon-rich sustainable material [16]. During the heat treatment process, metal oxides doped into the carbon matrix of biochar can be reduced to form carbides by reducing gases such as H_2, CO, and CH_4 *in situ* released from biochar. So, another part of this work is to test the feasibility to synthesize molybdenum carbide on biochar without using additional carbon sources or reducing gas and investigate its formation procedure.

This study was to synthesize molybdenum carbide by carburization of molybdenum salts on biochar in an inert gas such as argon and investigate the phase change during preparation. The CH_4 and/or CO_2 reactions on the catalyst surface were tested through temperature programmed surface reactions. Experiments were further conducted to evaluate the catalytic performance and stability.

2. Experimental

2.1. Biochar and pretreatment

The raw biochar was prepared by catalytic fast pyrolysis of loblolly pine sawdust and sieved into the particle size range of 0.18–0.25 mm, which was denoted as RBC. The RBC was further pretreated using nitric acid (HNO_3, Fisher Chemical, USA) to remove residual bio-oil and ash. The pretreatment was also to increase the number of surface oxygen-containing functional groups, which was useful for the metal deposition and dispersion [17]. Typically, 10 g RBC in 250 mL of 0.1 M HNO_3 solution was refluxed at 100 °C for 12 h. The biochar was then filtered and washed with hot deionized water to remove excess acid until the pH value was around 7. The treated biochar was then dried at 105 °C overnight. This product was used as the catalyst support and denoted as BC.

2.2. Preparation of biochar supported molybdenum carbide

Biochar supported molybdenum carbide was prepared by using the incipient wetness impregnation method [15] followed by carburization. Dried BC was impregnated with an aqueous solution of ammonium molybdate tetrahydrate $[(NH_4)_6Mo_7O_{24}{\cdot}4H_2O$, 99%, Sigma-Aldrich, USA) to load 15 wt% initial Mo on the BC. The obtained slurry was dried at a room temperature for 6 h and further dried at 105 °C overnight. The dried material was carburized in a tubular furnace at an atmospheric pressure purged with 100 mL/min argon (99.999% purity). The temperature was raised to 800 °C at 5 °C/min and subsequently held at 800 °C for 2 h. The material was cooled down to the ambient temperature in argon for characterization. The biochar supported molybdenum carbide was denoted as Mo_2C/BC.

2.3. Characterization

Phase formation during carburization was investigated using a Panalytical Empyrean X-ray diffractometer equipped with an Anton Parr HTK 1200 N high-temperature oven chamber (Boulder, CO, USA). A total of ~50 mg biochar supported ammonium molybdate powder was loaded into the chamber and heated from 25 °C to 800 °C at a heating rate of 3 °C/min in 20 mL/min helium. Diffraction patterns were measured using Cu-Kα X-ray radiation with a wavelength of 0.15418 nm and a 2θ range of 8°–65° 2θ. Each diffraction pattern was measured for 6 min using a step size and count time of 0.0262° 2θ and 43 s/step, respectively.

Thermogravimetry with evolved gas analysis (TGA-MS) for samples of biochar and biochar supported ammonium heptamolybdate were performed by using a TA SDT Q600 thermalgravimetric analyzer (New Castle, DE, USA) coupled to an Agilent 5975C mass spectrometer (Santa Clara, CA, USA), in which the sample was heated to 900 °C at a heating rate of 5 °C/min in 100 mL/min N_2.

X-ray powder diffraction (XRD) patterns for phase identification were obtained using an Agilent Gemini operated at 40 kV and 40 mA with Cu-Kα monochromatized radiation ($\lambda = 0.154056$ nm) (Santa Clara, CA, USA).

To obtain morphology of Mo_2C/BC at 800 °C, scanning electron microscopy (SEM) images were acquired on a JEOL JSM-7600F scanning electron microscope (Tokyo, Japan) operated at a 2 kV accelerating potential provided with an in-lens detector. Prior to the imaging, the sample was sputter coated with gold-palladium at 5 nm thickness. High-resolution transmission electron microscopy (HRTEM)

was applied by using a JEOL 2010F operated at 200 kV (Tokyo, Japan).

To compare surface area and pore size in samples of RBC, BC, and Mo_2C/BC, physical adsorption was measured with a Micromeritics ASAP 2020 surface area and porosity analyzer (Norcross, GA, USA). Elemental analyses for carbon, hydrogen, and nitrogen contents were determined by using a Perkin-Elmer 2400 CHN/S analyzer (Waltham, MA, USA). Mineral analysis was performed using a Varian 710-ES inductively coupled plasma optical emission spectrometer (ICP-OES) (Santa Clara, CA, USA).

Temperature programmed reactions over molybdenum carbides surface were carried out in a fixed-bed tubular stainless steel reactor at a heating rate of 10 °C/min in various gases. The production gases of CH_4, CO_2, CO, and H_2 were detected by the Agilent 5975C mass spectrometer (Santa Clara, CA, USA) connected online.

2.4. CO_2 reforming of CH_4 reaction

The CO_2 reforming of CH_4 reaction was performed in a fixed-bed continuous flow stainless steel tubular reactor with an inner diameter of 12.7 mm. The reaction was fed with CH_4/CO_2 mixture gases controlled by the mass flow meters (Brooks Instrument, USA) at 0.5 MPa controlled by a back-pressure regulator. The gas hourly space velocity (GHSV), defined as the ratio of the standard volumetric flow rate to the undiluted volume of catalyst, was varied between 4000 and 12,000 h^{-1}. The product stream from the reactor was passed to a gas-liquid separator, where the temperature was lowered to 0 °C using a coolant. The gas phase from the condenser was then passed through a wet test flow meter. The gases were analyzed by using an Agilent 7890 gas chromatograph (Santa Clara, CA, USA).

The conversion efficiencies of CH_4 (X_{CH4}) and CO_2 (X_{CO2}) were defined as moles of CH_4 and CO_2 converted per total moles of CH_4 and CO_2 according to Eqs. (1) and (2), respectively.

$$X_C H_4 = \frac{[CH_4]_{in} - [CH_4]_{out}}{[CH_4]_{in}} \times 100 \quad (1)$$

$$X_C O_2 = \frac{[CO_2]_{in} - [CO_2]_{out}}{[CO_2]_{in}} \times 100 \quad (2)$$

The ratio of H_2/CO was defined as Eq. (3):

$$H_2/CO = \frac{[H_2]_{ou}}{[CO]_{out}} \quad (3)$$

3. Results and discussion

3.1. Biochar pretreatment

The pretreatment of the RBC with HNO_3 could effectively remove alkali metals such as Na and K, alkaline earth metals such as Mg and Ca, and other metals such as Al and Mn (Table S1). However, the content of Si did not decrease because HNO_3 cannot dissolve SiO_2. The pretreatment of the RBC with HNO_3 increased the surface area of the biochar from 627 to 768 m^2/g and the pore volume from 0.42 to 0.51 cm^3/g (Table 2). The BC had a carbon content of 85.1 wt%, which was slightly lower than 87.2 wt% in the RBC due to the removal of bio-oil residue.

3.2. Molybdenum carbide formation during carburization

The formation of molybdenum carbide from ammonium molybdate in an inert gas was investigated by using *in-situ* XRD and TGA-MS. Carburization from ammonium molybdate to molybdenum carbide on biochar was explicitly demonstrated by *in-situ* XRD as shown in Fig. 1. The first pattern recorded at 25 °C exhibited ammonium molybdenum oxide $(NH_4)_2Mo_3O_{10}$ phase (PDF 79-1905), which was produced during the drying process of the biochar supported ammonium molybdate $(NH_4)_2Mo_7O_{24}{\cdot}4H_2O$ at 105 °C. The intermediate phase of

Table 2
Elemental and physical properties analysis results.

Sample	RBC	BC	Mo_2C/BC
C[a] (wt%)	87.2	85.1	69.2
H[a] (wt%)	1.7	1.9	0.7
N[a] (wt%)	0.6	0.7	0.5
Mo[b] (wt%)	0	0	19.5
BET[c] (m^2/g)	627	768	404
Pore Diameter [d] (nm)	5.78	5.86	7.91
Pore Volume[e] (cm^3/g)	0.42	0.51	0.28

[a] Measured with Perkin-Elmer 2400 CHN/S analyzer.
[b] ICP.
[c] Brunauer-Emmet-Teller (BET) surface area.
[d] pore diameter calculated by the Barrett-Joyner-Halenda (BJH) method using adsorption branches.
[e] Total pore volume calculated as the amount of nitrogen adsorbed at a relative pressure of 0.995.

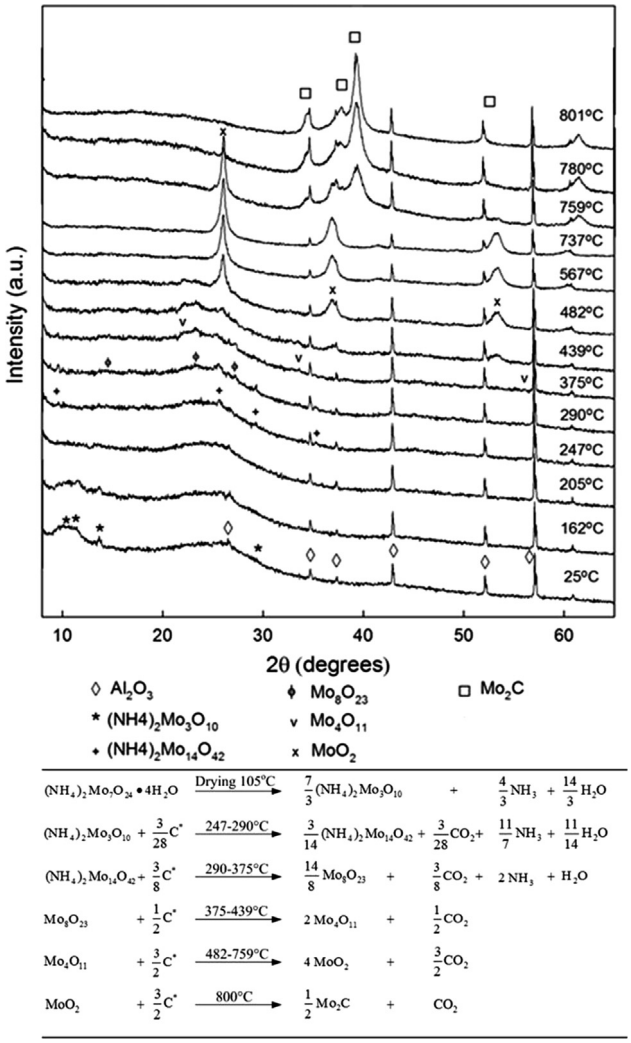

Fig. 1. *In-situ* XRD results from carburization of biochar supported ammonium molybdate from 25 to 800 °C at 3 °C/min in 20 mL/min helium. Active phase was denoted as C*.

$(NH_4)_2Mo_{14}O_{42}$ (PDF 26-0079) during decomposition was detected between 247 and 290 °C. The intermediate phase was further reduced to Mo_8O_{23} (PDF 05-0339) between 290 and 375 °C, and Mo_4O_{11} (PDF 05-0337) or (PDF 13-0142) between 375 and 439 °C. A monoclinic MoO_2 (PDF 32-0671) phase occurred at 482 °C, began to decrease at 759 °C, and disappeared at 801 °C. At the same time, a hexagonal (hcp)

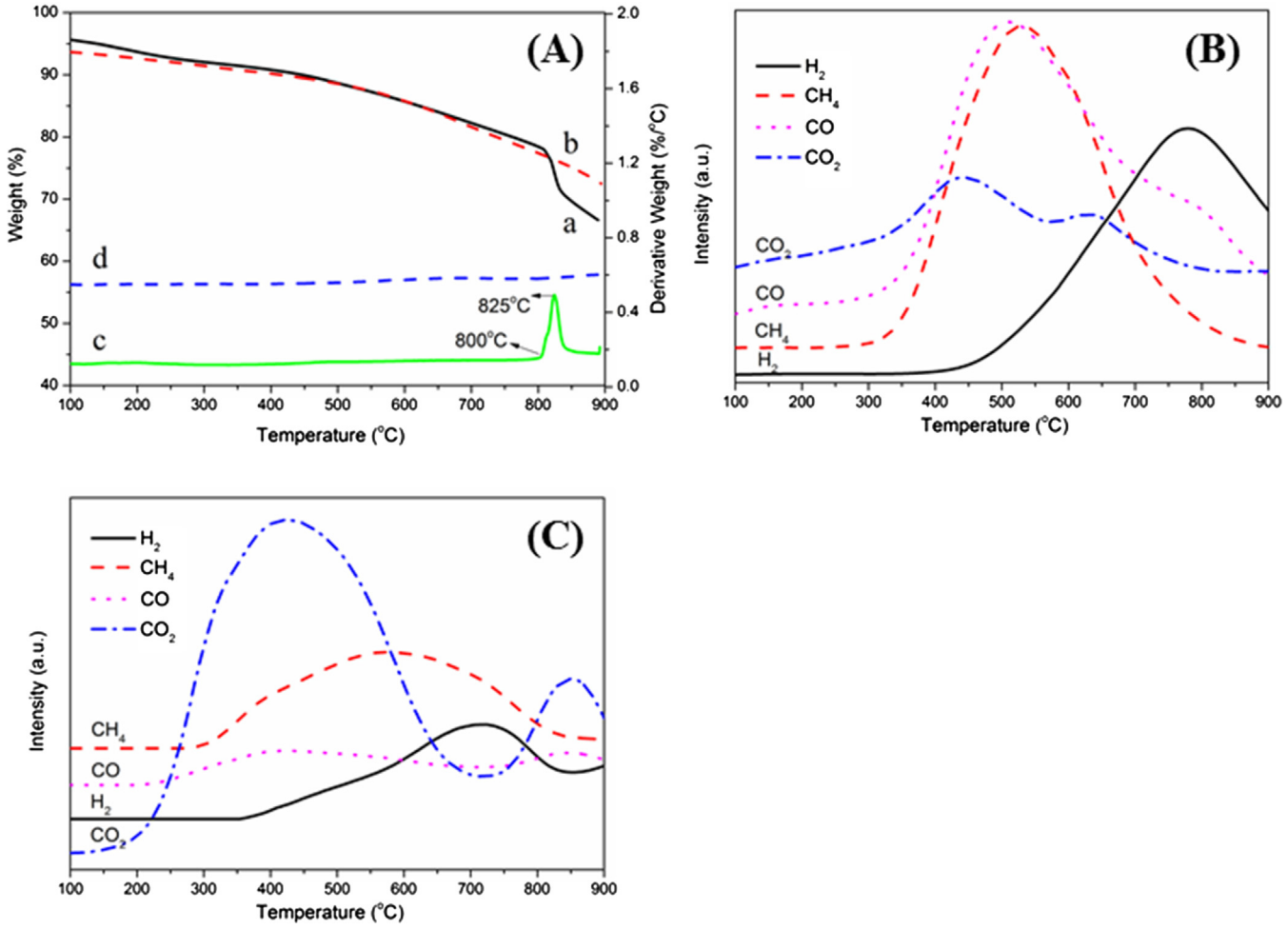

Fig. 2. TGA-MS. (A) TGA analyses of biochar supported ammonium heptamolybdate (a) and biochar (b), and DTG plots of biochar supported ammonium heptamolybdate (c) and biochar (d). Mass spectra profiles of evolved gases from biochar (B) and biochar supported ammonium molybdate (C).

β-Mo_2C (PDF 35-0787) phase started to form.

The thermal decomposition behaviors of biochar supported ammonium heptamolybdate and biochar were compared in nitrogen as shown in Fig. 2A. In Fig. 2Ab, the continuous gradual weight loss of biochar was 27.7 wt% during the heating procedure to 900 °C, which was caused by the evolution of gaseous species such as H_2, CO, CO_2, and CH_4 were evolved. In Fig. 2B, the corresponding peak temperatures of CO desorption centered at 500 °C, the CH_4 desorption centered at 530 °C, the H_2 desorption centered at 770 °C, and the CO_2 desorption centered at 430 °C and 640 °C. The biochar supported ammonium heptamolybdate showed a weight loss between 350 and 800 °C (Fig. 2Aa), which corresponded to the reduction of ammonium heptamolybdate to MoO_2 by reducing gases released from biochar. The sharp peak around 825 °C was attributed to the formation of molybdenum carbide (Fig. 2Ac). Fig. 2C exhibited gases change after interaction with molybdenum species during the carburization process. Compared with the result of biochar, the more CO_2 evolution from biochar supported molybdenum compounds between 100 and 750 °C could be attributed to the resulting CO_2 during molybdenum species were reduced. This CO_2 evolution was accompanied by the CO consumption, which indicated that CO was one of active agent for molybdenum species reduction. The second CO_2 evolution peak around 840 °C indicated that carbon source in molybdenum carbide might come from a solid carbon activated at 800 °C. The H_2 exhausted from 400 to 900 °C, which indicated that H_2 was another possible active agent for the molybdenum species reduction. The CH_4 profile did change significantly between 300 and 800 °C, which indicated that CH_4 also worked as an active agent.

From both *in-situ* XRD and TGA-MS results, the molybdenum carbide formation pathway involved the sequencing process: $(NH_4)_6Mo_7O_{24}{\cdot}4H_2O \rightarrow (NH_4)_2Mo_3O_{10} \rightarrow (NH_4)_2Mo_{14}O_{42} \rightarrow Mo_8O_{23} \rightarrow Mo_4O_{11} \rightarrow MoO_2 \rightarrow Mo_2C$. Both the volatile gases CO, H_2, and CH_4 released from biochar and the biochar solid carbon participated in molybdenum species reduction. Both biochar and CH_4 may act as the carbon sources for carbide formation.

3.3. Characterization of biochar supported molybdenum carbide

The HRTEM image in Fig. 3A indicated that molybdenum carbide particles (darker nanoparticles) were embedded in an amorphous carbon matrix. Their size ranged from 6 to 20 nm with an average diameter of 12 nm when carburized at 800 °C for 2 h. XRD patterns of biochar supported ammonium molybdate and its carburized products Mo_2C/BC at 800 °C and 900 °C for 2 h were compared as shown in Fig. S2. The carburized products showed the hexagonal β-Mo_2C phase (PDF 35-0787), where 2θ peaks located at 39.6° (1 0 1), 37.8° (0 0 2), 52.3° (1 0 2), 34.4° (1 0 0), 61.5° (1 1 0), 69.8° (1 0 3), and 74.5° (1 1 2). Fig. 3B shows the d-spacing values of 0.228 nm for the (1 0 1) crystallographic planes. The average crystallite size was 9.8 nm at 800 °C and 10.7 nm at 900 °C determined by (1 0 1) peak using Scherrer formula. Molybdenum carbide crystallite size increased with the increased temperature. The SEM image shows that biochar has a ~100 nm vessel structure (Fig. S3a), which may be created during the catalytic pyrolysis process. It was rare to observe metal particles deposited on the biochar surface (Fig. S3b), which indicated that most metal particles might

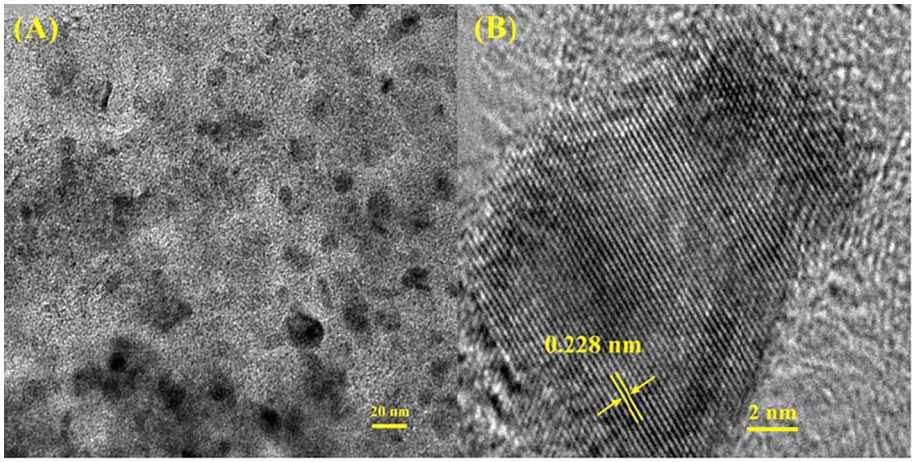

Fig. 3. HRTEM images of Mo_2C/BC at 800 °C.

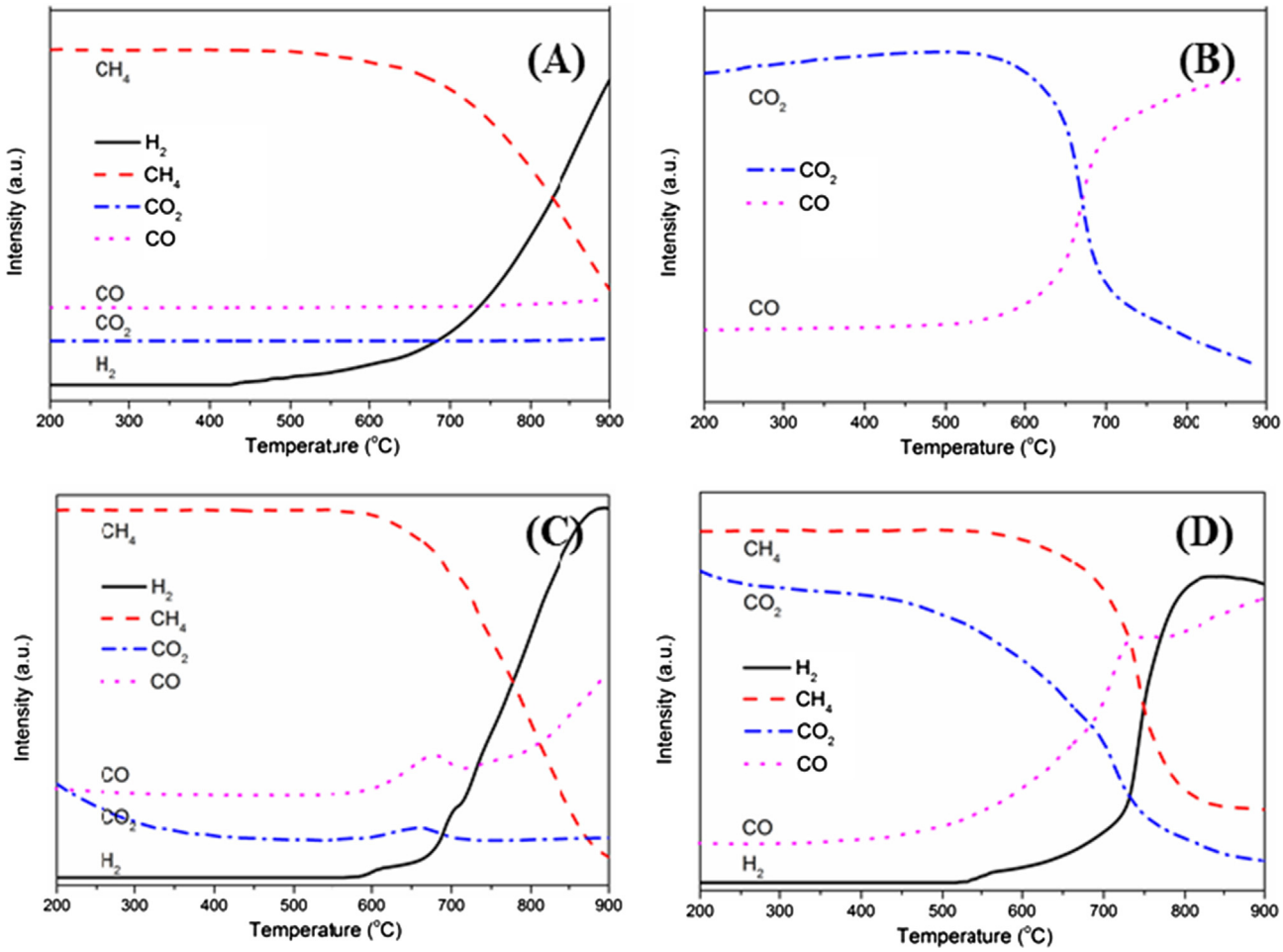

Fig. 4. Temperature programmed surface reactions of Mo_2C/BC. (A) reaction with CH_4, (B) reaction with CO_2, (C) the sample of (B) reacted with CH_4, (D) reaction in the CO_2 reforming of CH_4.

infiltrate into the channels of biochar.

The CHN and ICP analyses revealed that the contents of C, Mo, H, and N in Mo_2C/BC (initial 15 wt% Mo loading) were 69.2%, 19.5%, 0.7%, and 0.5%, respectively (Table 2). The loading of Mo particles blocked the pores within the carbon matrix, which caused the reduction of surface area from 768 to 404 m^2/g and a pore volume from 0.51 to 0.28 m^3/g, and the average pore diameter increased from 5.86 to 7.91 nm.

3.4. Temperature programmed surface reactions

In Fig. 4A, CO_2, CH_4, CO, and H_2 were recorded while the Mo_2C was heated to 900 °C in 10 mL/min CH_4. CH_4 consumed along with the H_2 formation over about 630 °C and CH_4 dissociation reached a maximum value at 850 °C (Fig. S4A). The generation of H_2 and disappeared CO indicated that CH_4 dissociated as $CH_4 \rightleftharpoons C* + 2H_2$ on the catalyst surface. Deposited graphitic carbon (PDF 41–1487) with 2θ peaks at

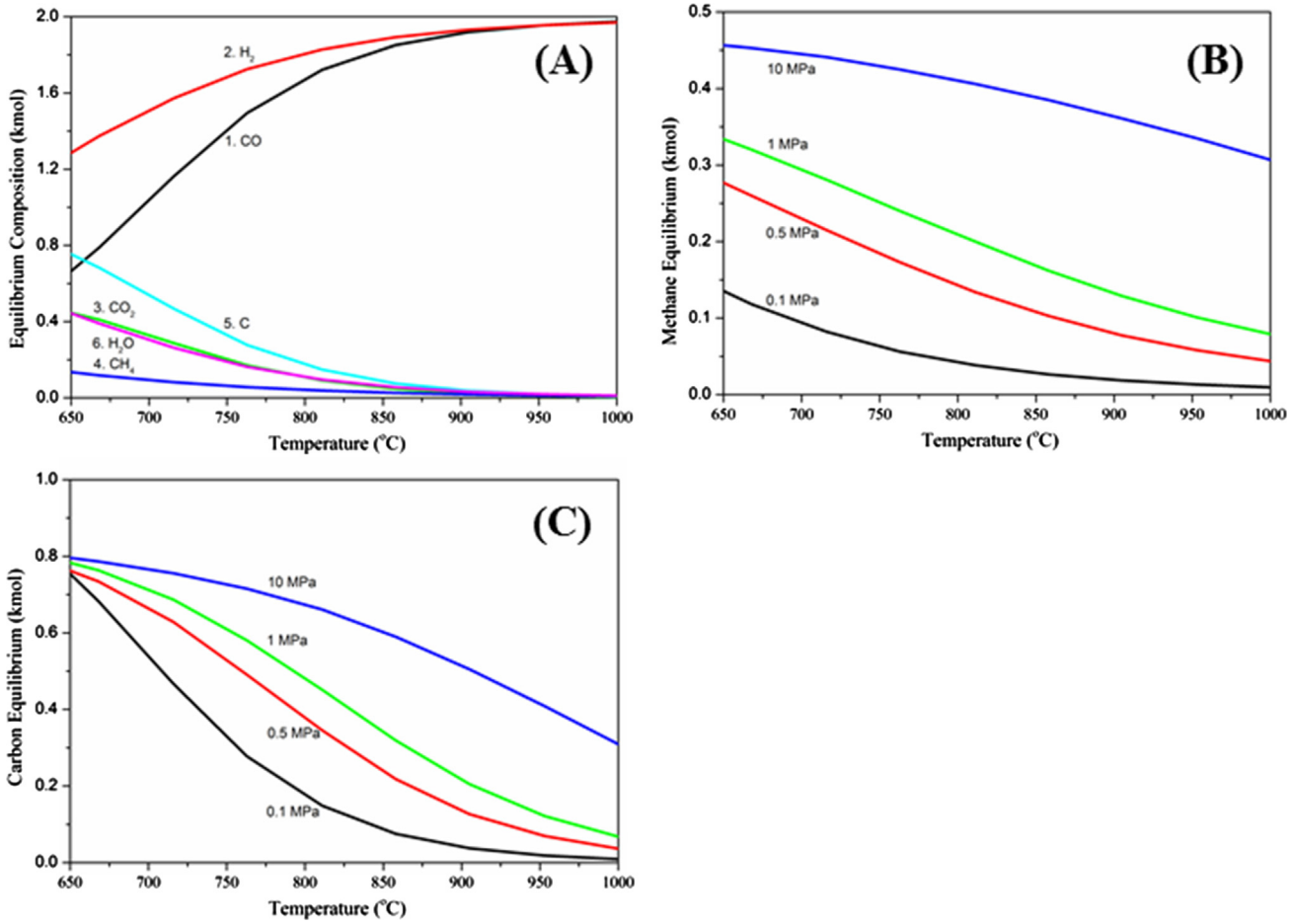

Fig. 5. (A) The equilibrium composition with the temperature at 0.1 MPa with a CH_4/CO_2 mole ratio of 1. The effect of pressure on the methane conversion (B) and carbon formation (C) as a function of temperature at (1) 0.1 MPa, (2) 0.5 MPa, (3) 1 MPa, and (4) 10 MPa with a CH_4/CO_2 mole ratio of 1.

26.1° (0 0 2), 42.7° (1 0 0), and 44.4° (1 0 1) was confirmed by XRD (Fig. 6Dc). The CO_2 oxidation of Mo2C was investigated by temperature programmed reaction in 10 mL/min CO_2 flow (Fig. 4B). The only generation CO occurred ~668 °C (Fig. S4B), indicated that CO_2 acted as $CO_2 + C* \leftrightharpoons 2CO + *$ due to oxidation of Mo_2C to Mo oxide species [18,19]. The sample after reaction with CO_2 at 900 °C was cooled down to a room temperature in 10 mL/min CO_2, and then the sample was heated up to 900 °C in 10 mL/min CH_4 shown in Fig. 4C. The only reactant CH_4 started to decrease at ~600 °C accompanied by the formation of CO and H_2. The maximum consumption of CH_4 was at 690, 730, and 805 °C (Fig. S4C). This indicated that CH_4 acted as a reductant to reduce molybdenum species to oxy-carbides or carbide species [20,21].

The reaction in the CO_2 reforming of CH_4 was studied, in which Mo_2C/BC was heated up to 900 °C in a mixture of 10 mL/min CH_4 and 10 mL/min CO_2. The results showed that CO_2 and CH_4 responded starting at 450 and 550 °C (Fig. 4D) and their maximum consumption at 710 and 740 °C (Fig. S4D), respectively.

3.5. Thermodynamic analysis

To predict possible reaction conditions for DRM, the thermodynamic equilibrium products' distribution including carbon formation as a function of temperature were performed using HSC Chemistry 6.0 Software. These mole compositions were calculated using Gibbs free energy minimization simulations. These simulations were performed by assuming an initial equimolar mixture of $CH_{4\ (g)}$ and $CO_{2\ (g)}$ and including $H_{2(g)}$, $CO_{(g)}$, $H_2O_{(g)}$, and $C_{(s)}$ as products in the calculation. Solid carbon $C_{(s)}$ was regarded as graphite in the reforming process [22]. Fig. 5A showed the effect of temperature on the CO_2 reforming of CH_4 based on 1 kmol each of CH4 and CO2 over a temperature range of 650–1000 °C, and at a constant pressure of at 0.1 MPa. The conversion of CH4 and CO2 increased with the increased temperature. The yield of H_2 and CO increased with the increased temperature·H_2O diminished with increasing temperature. The reasonable conversions should be performed at 850 °C. The effect of pressure on CO_2 reforming of CH_4 reaction was indicated by methane conversion with a CH_4/CO_2 mole ratio of 1 at 0.1 MPa, 0.5 MPa, 1 MPa, and 10 MPa (Fig. 5B). The methane conversion decreased with increased pressure. At 850 °C, the methane conversion was reasonable at pressures below 0.5 MPa.

The carbon formation is a major concern, because it can deactivate the catalyst and lower the performance. It is important to predict carbon formation conditions to minimize carbon formation by optimizing the operation conditions. At 0.1 MPa, carbon formation decreased with increased temperature, especially in the temperature range of 550–700 °C (Fig. 5A). Although carbon deposit mainly comes from Boudouard reaction and methane decomposition, the exothermic Boudouard reaction is favored at low temperature and prohibited by the increased temperature, and ceases over 700 °C. The effect of pressure on solid carbon formation was simulated with a CH_4/CO_2 mole ratio of 1 at 0.1 MPa, 0.5 MPa, 1 MPa, and 10 MPa. Carbon deposition decreased with the decreased pressure from 10 to 0.1 MPa (Fig. 5C).

3.6. Catalytic performance for CO_2 reforming of CH_4 to syngas

The temperature effect on CO_2 reforming of CH_4 performance over the catalyst was indicated by the conversion of CH_4 and CO_2, and the

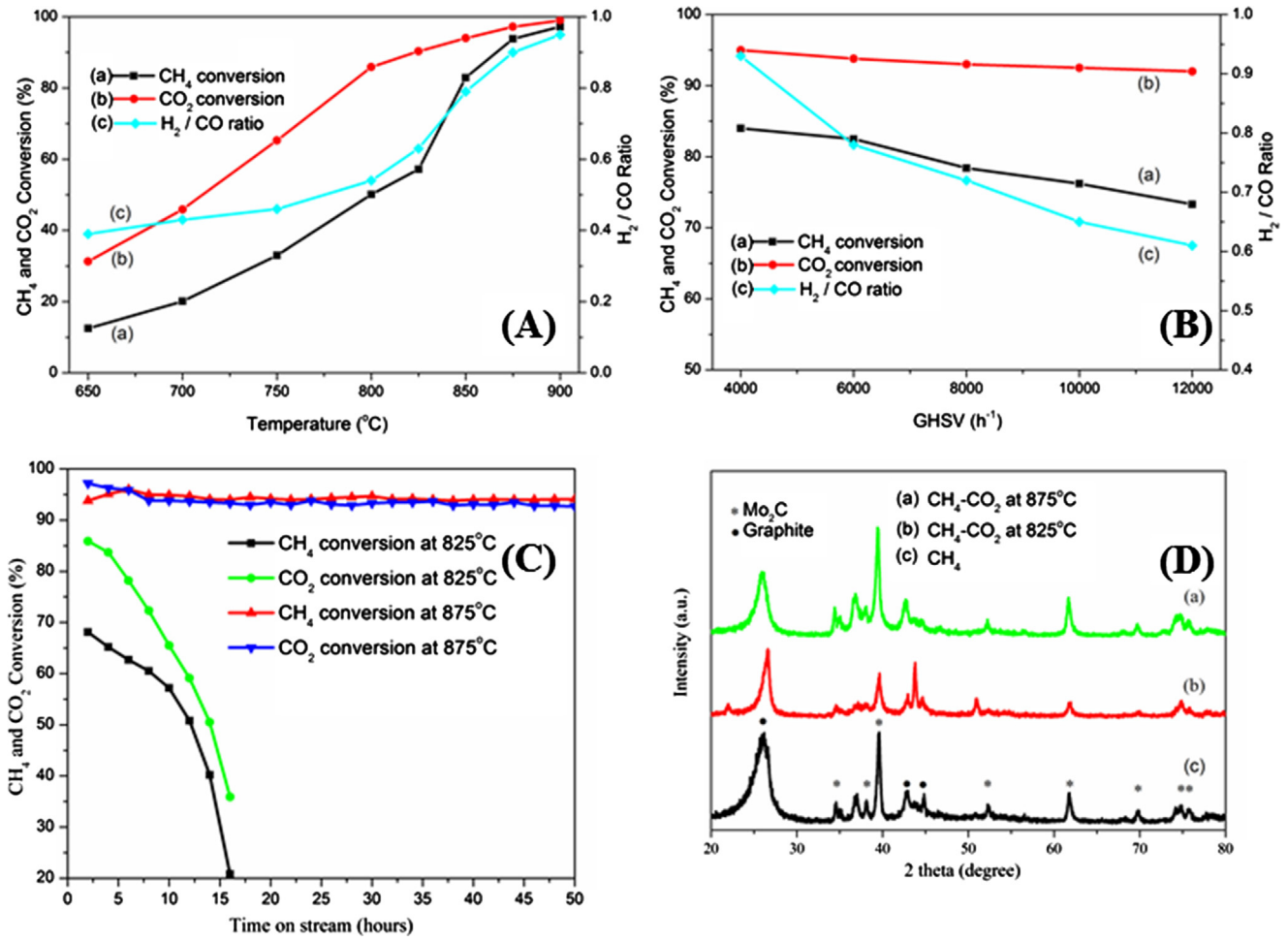

Fig. 6. (A) The effect of temperature on the CH_4 conversion, CO_2 conversion, and H_2/CO ratio. (Conditions: CH_4/CO_2 ratio of 1, GHSV of 6000 h^{-1}). (B) The effect of GHSV on the CH_4 conversion, CO_2 conversion, and H_2/CO ratio. (Conditions: CH_4/CO_2 ratio of 1, GHSV of 4000–12,000 h^{-1}, 850 °C). (C) A lifetime study of the catalyst for the CO_2 reforming of CH_4 reaction. (Conditions: at 825 and 875 °C, CH_4/CO_2 ratio of 1, GHSV of 6000 h^{-1}). (D) XRD patterns of catalyst Mo_2C/BC (a) CH_4 and CO_2 at 875 °C. (b) CH_4 and CO_2 at 825 °C, and (c) CH_4.

selectivity was expressed in terms of the H_2/CO ratio (Fig. 6A). Both CH_4 and CO_2 conversion increased with the increased temperature. The high temperature increases the conversion, because the CO_2 reforming of CH_4 reaction is a strongly endothermic reaction. The CH_4 conversion increased from 12.8% to 97.2% and the CO_2 conversion increased from 20.5% to 99.0% between 650 and 900 °C. When the temperature reached 850 °C, CH_4 conversion rapidly exceeded 90%. The CO_2 conversion was always higher than that of CH_4 and the H_2/CO ratio was lower than unity between 650 and 900 °C, which revealed that the reverse water-gas shift reaction occurred with consuming H_2 and producing CO.

The effect of GHSV on the CH_4 conversion, CO_2 conversion, and the H_2/CO ratio at 850 °C was shown in Fig. 6B. The CH_4 conversion, CO_2 conversion, and H_2/CO ratio decreased with increased GHSV. The CH_4 conversion, CO_2 conversion, and H_2/CO ratio decreased from 83.9% to 73.3%, 95.0% to 92.0%, and 0.93 to 0.61, respectively, when the GHSV increased from 4000 to 12,000 h^{-1}. CO_2 conversion dropped more slowly than CH_4 conversion, which indicated that the reaction of CO_2 with the catalyst was more favorable than that of CH_4 with the catalyst.

Temperature tests indicated that both CH_4 and CO_2 conversions were higher than 80% at 850 °C with the GHSV of 6000 h^{-1} (Fig. 6A). To compare the stability of Mo_2C above and below 850 °C, two stability tests were carried out at 825 °C and 875 °C, respectively. In Fig. 6C, the conversions of CO_2 and CH_4 stabilized at 97% and 94%, respectively, at 875 °C during the 50-h test, and no decay of activity was found. The catalyst reacted at 875 °C still has XRD 2θ peaks belonged to Mo_2C in Fig. 6 Da. The conversions of CO_2 and CH_4 were clearly decreased at 825 °C, reflecting gradual catalyst deactivation. After the catalyst reacted at 825 °C, XRD results exhibited 2θ peaks at 22.0°, 26.6°, 43.8°, and 51.0° (Fig. 6Db).

4. Conclusions

Biochar supported molybdenum carbide nanoparticles ranging from 6 to 20 nm were efficiently synthesized using the incipient wetness impregnation method followed by the carburization in an inert gas. The usage of reducing gas like CH_4 and H_2 is not necessary for carburization, and thus the synthesis process was simplified and the cost can be reduced. Both the volatile gases released from biochar and the biochar solid carbon participated in reduction and carbonization process. Temperature programmed surface reactions indicated that CH_4 dissociated as $CH_4 \leftrightharpoons C* + 2H_2$ on the catalyst surface, and CO_2 reacted as $CO_2 + C* \leftrightharpoons 2CO + *$ due to oxidation of Mo_2C. The carbon deposition decreased with the decreased pressure and decreased with increased temperature, which mainly comes from methane decomposition at 850 °C. Both experiment data and thermodynamic analysis for CO_2 reforming of CH_4 clearly demonstrated that the conversion of CH4 and CO2 increased with the increased temperature, the yield of H_2 and CO increased with the increased temperature, and the reasonable conversion should be performed at ~850 °C. At 875 °C, 0.5 MPa, and 6000 h^{-1}, CH_4 and CO_2 conversions were 94% and 97%, respectively.

Acknowledgments

This work was partially supported by United States NSF-CREST Center for Bioenergy [Award No. HRD-1242152], United States Department of Energy [Award No. EE0003138], United States Department of Agriculture (USDA-NIFA) [Award No. NC.X-303-5-17-130-1], and United States Department of Agriculture (USDA-NIFA) [Award No. NC.X-314-5-18-130-1].

Appendix A. Supplementary data

Supplementary data associated with this article can be found, in the online version, at http://dx.doi.org/10.1016/j.fuel.2018.03.179.

References

[1] Dai C, Zhang S, Zhang A, Song C, Shi C, Guo X. Hollow zeolite encapsulated Ni-Pt bimetals for sintering and coking resistant dry reforming of methane. J Mater Chem A 2015;3(32):16461–8.
[2] Shekhawat II D, Spivey JJ, Berry DA. Fuel cells: technologies for fuel processing. Elsevier; 2011.
[3] Claridge JB, York APE, Brungs AJ, Marquez-Alvarez C, Sloan J, Tsang SC, et al. New Catalysts for the Conversion of Methane to Synthesis Gas: Molybdenum and Tungsten Carbide. J Catal 1998;180(1):85–100.
[4] York APE, Claridge JB, Márquez-Alvarez C, Brungs AJ, Tsang SC, Green MLH. Synthesis of early transition metal carbides and their application for the reforming of methane to synthesis gas. In: R.K. Grasselli STOAMG, Lyons JE, editors. Studies in Surface Science and Catalysis. Elsevier; 1997, p. 711–20.
[5] Ross JRH. Natural gas reforming and CO2 mitigation. Catal Today 2005;100(1–2):151–8.
[6] Porosoff MD, Yang X, Boscoboinik JA, Chen JG. Molybdenum Carbide as Alternative Catalysts to Precious Metals for Highly Selective Reduction of CO2 to CO. Angew Chem 2014;126(26):6823–7.
[7] Li R, Shahbazi A, Wang L, Zhang B, Hung AM, Dayton DC. Graphite encapsulated molybdenum carbide core/shell nanocomposite for highly selective conversion of guaiacol to phenolic compounds in methanol. Appl Catal A 2016;528:123–30.
[8] LaMont DC, Thomson WJ. Dry reforming kinetics over a bulk molybdenum carbide catalyst. Chem Eng Sci 2005;60(13):3553–9.
[9] Xiao T-c, Hanif A, York APE, Nishizaka Y, Green MLH. Study on the mechanism of partial oxidation of methane to synthesis gas over molybdenum carbide catalyst. Phys Chem Chem Phys 2002;4(18):4549–54.
[10] Gao H, Yao Z, Shi Y, Wang S. Improvement of the catalytic stability of molybdenum carbide via encapsulation within carbon nanotubes in dry methane reforming. Catal Sci Technol 2018;8(3):697–701.
[11] Chen WF, Wang CH, Sasaki K, Marinkovic N, Xu W, Muckerman JT, et al. Highly active and durable nanostructured molybdenum carbide electrocatalysts for hydrogen production. Energy Environ Sci 2013;6(3):943–51.
[12] Kaewpanha M, Guan G, Ma Y, Hao X, Zhang Z, Reubroychareon P, et al. Hydrogen production by steam reforming of biomass tar over biomass char supported molybdenum carbide catalyst. Int J Hydrogen Energy 2015;40(25):7974–82.
[13] Wang Y-Y, Ling L-L, Jiang H. Selective hydrogenation of lignin to produce chemical commodities by using a biochar supported Ni-Mo2C catalyst obtained from biomass. Green Chem 2016;18(14):4032–41.
[14] Yan Q, Lu Y, To F, Li Y, Yu F. Synthesis of tungsten carbide nanoparticles in biochar matrix as a catalyst for dry reforming of methane to syngas. Catal Sci Technol 2015;5(6):3270–80.
[15] Yan Q, Wan C, Liu J, Gao J, Yu F, Zhang J, et al. Iron nanoparticles in situ encapsulated in biochar-based carbon as an effective catalyst for the conversion of biomass-derived syngas to liquid hydrocarbons. Green Chem 2013;15(6):1631–40.
[16] Xiu S, Shahbazi A, Li R. Characterization, Modification and Application of Biochar for Energy Storage and Catalysis: A Review. Trends Renew Energy 2017;3(1):86–101.
[17] Zhou X, Ji J, Wang D, Duan X, Qian G, Chen D, et al. Hierarchical structured [small alpha]-Al2O3 supported S-promoted Fe catalysts for direct conversion of syngas to lower olefins. Chem Commun 2015;51(42):8853–6.
[18] Darujati ARS, LaMont DC, Thomson WJ. Oxidation stability of Mo2C catalysts under fuel reforming conditions. Appl Catal A 2003;253(2):397–407.
[19] LaMont DC, Thomson WJ. The influence of mass transfer conditions on the stability of molybdenum carbide for dry methane reforming. Appl Catal A 2004;274(1):173–8.
[20] Lacheen HS, Iglesia E. Stability, structure, and oxidation state of Mo/H-ZSM-5 catalysts during reactions of CH4 and CH4–CO2 mixtures. J Catal 2005;230(1):173–85.
[21] Zheng H, Ma D, Bao X, Hu JZ, Kwak JH, Wang Y, et al. Direct Observation of the Active Center for Methane Dehydroaromatization Using an Ultrahigh Field 95Mo NMR Spectroscopy. J Am Chem Soc 2008;130(12):3722–3.
[22] Bradford MCJ, Vannice MA. CO2 Reforming of CH4. Catal Rev 1999;41(1):1–42.